

Electrocatalysis

International Edition: DOI: 10.1002/anie.201701149
German Edition: DOI: 10.1002/ange.201701149

Highly Branched Metal Alloy Networks with Superior Activities for the Methanol Oxidation Reaction

Xun Cui, Peng Xiao, Jing Wang, Ming Zhou, Wenlong Guo, Yang Yang, Yanjie He, Zewei Wang, Yingkui Yang, Yunhuai Zhang,* and Zhiqun Lin*

Abstract: Three-dimensional (3D) interconnected metal alloy nanostructures possess superior catalytic performance owing to their advantageous characteristics, including improved catalytic activity, corrosion resistance, and stability. Hierarchically structured Ni-Cu alloys composed of 3D network-like microscopic branches with nanoscopic dendritic feelers on each branch were crafted by a facile and efficient hydrogen evolution-assisted electrodeposition approach. They were subsequently exploited for methanol electrooxidation in alkaline media. Among three hierarchically structured Ni-Cu alloys with different Ni/Cu ratios ($Ni_{0.25}Cu_{0.75}$, $Ni_{0.50}Cu_{0.50}$, and $Ni_{0.75}Cu_{0.25}$), the $Ni_{0.75}Cu_{0.25}$ electrode exhibited the fastest electrochemical response and highest electrocatalytic activity toward methanol oxidation. The markedly enhanced performance of $Ni_{0.75}Cu_{0.25}$ electrocatalyst can be attributed to its alloyed structure with the proper Ni/Cu ratio and a large number of active sites on the surface of hierarchical structures.

Direct methanol fuel cells (DMFCs) are widely recognized as an emerging power source for portable electronic devices and electric vehicles.^[1] To improve the kinetics of methanol oxidation reaction (MOR), much work has focused on the development of efficient electrocatalysts.^[2] To date, various low-cost non-noble metals as alternative catalysts to the noble metal counterparts have been investigated, especially Ni-based metals owing to their high catalytic activity and low cost.^[3] In general, the chemical composition and surface structure are key in determining the performance of electrocatalysts as the catalytic reaction usually occurs on their surface. In this context, several approaches have been

developed to improve the catalytic performance of Ni-based electrocatalysts.

The first approach involves the addition of a second metal to Ni-based electrocatalysts, such as the transition metals Co, Cu, and Mn^[4] for MOR. When compared with the monometallic electrocatalyst for methanol oxidation, the enhanced activity of the resulting bimetallic electrocatalysts can be ascribed to both the bi-functional mechanism and the alloy-induced electronic effect.^[5] Furthermore, theoretical studies have revealed the modification of electronic structure of bimetallic clusters owing to the charge transfer between the binary atoms, thereby leading to a weakened CO adsorption on the binary cluster than on monometal itself.^[6]

As the second approach, the catalyst support is commonly used for Ni-based metals during the MOR process. Recently, carbon nanofiber and graphene have been incorporated in Ni-based bimetallic electrocatalysts for MOR.^[3c,4b] However, in such designs, the Ni-based metals are usually either simply weakly adsorbed on carbon or relatively strongly anchored on surface-functionalized carbon. For the former case, the tendency for nanoparticles to agglomerate under the operating condition over a long period of time hampers its potential applications.^[7] On the other hand, for the latter case, the surface-functionalized carbon substrates clearly make them more vulnerable to be excessively oxidized and become easily corroded under harsh operation condition of fuel cells, and ultimately result in a structural collapse and a rapid decay of electrochemical performance.^[8]

The third approach invokes the introduction of porous structures in electrocatalysts for fast and efficient transport through high surface area porous frameworks in MOR.^[9] Among various porous structures, hierarchical structure with a branched architecture have received considerable attention owing to intrinsic surface properties such as large surface-to-volume ratio, high surface roughness, and a large number of multiple high angle edges and sharp tips.^[10] These unique features enable them for high-performance advanced materials, particularly for catalysts.^[11] In electrocatalysis materials, the active sites are often located in micro- and mesopores, while the macro-pores promote the facile diffusion of species toward and away from the active sites.^[12] Moreover, the presence of these three different pore sizes results in large surface areas and short electron and ion transport paths, leading to enhanced catalytic activity.^[12] Much effort has been devoted to branched noble metal nanoarchitectures (for example, Pt, Au, Pd, and bimetallic species) for electrocatalysis.^[11,13] In contrast, the use of branched non-noble metal-based architectures as electrocatalysts is comparatively few and limited in scope.

[*] X. Cui, Prof. P. Xiao, J. Wang, M. Zhou, W. Guo, Y. Yang, Prof. Y. Zhang
College of Chemistry and Chemical Engineering
Chongqing University, Chongqing 400044 (China)
E-mail: xp2031@163.com

X. Cui, J. Wang, M. Zhou, Y. He, Z. Wang, Prof. Z. Lin
School of Materials Science and Engineering
Georgia Institute of Technology
Atlanta, GA 30332 (USA)
E-mail: zhiqun.lin@mse.gatech.edu

Prof. P. Xiao
College of Physics, Chongqing University
Chongqing 400044 (China)

Prof. Y. Yang
School of Materials Science and Engineering
South-Central University for Nationalities
Wuhan 430074 (China)

Supporting information and the ORCID identification number(s) for the author(s) of this article can be found under:
<http://dx.doi.org/10.1002/anie.201701149>.

Herein, we report a viable hydrogen evolution-assisted electrodeposition route to crafting hierarchically structured Ni-Cu alloy networks for methanol electrooxidation in alkaline media with markedly enhanced electrocatalytic performance. The hierarchical Ni-Cu alloy networks comprise interconnected branches at the microscopic scale in 3D and dendritic feelers at the nanometer scale within each microscopic branch. These hierarchically arranged Ni-Cu alloys possess a large volume of empty space (that is, a highly porous architecture) between them and exhibited excellent electrocatalytic properties. Among the three hierarchically structured Ni-Cu alloy networks produced ($\text{Ni}_{0.25}\text{Cu}_{0.75}$, $\text{Ni}_{0.50}\text{Cu}_{0.50}$ and $\text{Ni}_{0.75}\text{Cu}_{0.25}$), $\text{Ni}_{0.75}\text{Cu}_{0.25}$ alloys with a higher Ni content exhibited the highest electrocatalytic activity for MOR. The largely improved performance of $\text{Ni}_{0.75}\text{Cu}_{0.25}$ electrocatalyst may be due to its alloyed structure with the proper Ni/Cu ratio and a large number of active sites on the surface of hierarchical structures. This hydrogen evolution-assisted electrodeposition strategy is of practical interest for the development of low-cost Ni-based porous alloyed electrocatalysts.

Field-emission scanning electron microscopy (FESEM) images of as-prepared hierarchically structured Ni-Cu alloy networks obtained by electrodeposition (see the Experimental Section in the Supporting Information) are shown in Figure 1 a,b (see also the Supporting Information, Figure S1). A further scrutiny revealed that the deposited Ni-Cu alloys on the surface of Ti substrate displayed a structural hierarchy (Figure 1 a; Supporting Information, Figure S1 a,b), namely, microscopic interconnected branches forming a network at the microscopic scale in conjunction with the dendritic feelers at the nanometer scale within each branch. Moreover, Figure 1 b and Figure S1 c,d in the Supporting Information show that Ti substrates are uniformly covered by these hierarchically structured Ni-Cu alloys. Notably, the morphology of hierarchically structured Ni-Cu alloys with the different Ni/Cu ratios was very similar, indicating that the change of the molar ratios of Ni/Cu precursors had negligible effect on the morphology of final products. Further scrutiny of these Ni-Cu alloy networks by transmission electron microscopy (TEM) revealed a hierarchical structure (Figure 1 c,d; Supporting Information, Figure S2). The lattice fringes with an interplanar distance of 0.205 nm was found (insets in Figure 1 d), correlating well to the (111) plane of Ni-Cu alloy. The corresponding hierarchical structures are polycrystalline as demonstrated by the presence of diffraction rings (selected area electron diffraction pattern in Figure 1 d). The phase and composition of hierarchically structured Ni-Cu alloy networks were also examined by X-ray diffraction (XRD; Supporting Information, Figure S3), energy-dispersive X-ray spectroscopy (EDX) (Supporting Information, Figures S4, S5), and X-ray photoelectron spectroscopy (XPS; Figure 1 e,f; Supporting Information, Figure S6). Table S1 in the Supporting Information summarizes the actual atomic ratio and nominal atomic ratio of Ni: Cu of 0.73:0.27 and 0.75:0.25 for $\text{Ni}_{0.75}\text{Cu}_{0.25}$, 0.52:0.48 and 0.50:0.50 for $\text{Ni}_{0.50}\text{Cu}_{0.50}$, and 0.26:0.74 and 0.25:0.75 for $\text{Ni}_{0.25}\text{Cu}_{0.75}$, respectively. The EDX mapping (Supporting Information, Figure S7) revealed that the elemental distributions of Ni and Cu are uniform for

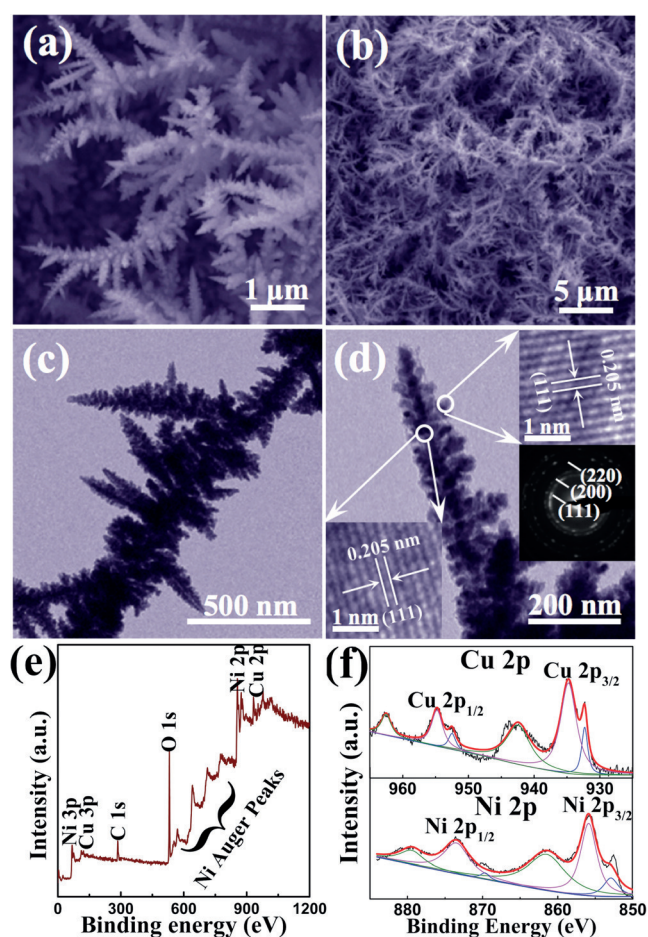


Figure 1. a),b) FESEM images and c),d) TEM images. e) XPS full spectra, and f) XPS survey of Cu 2p and Ni 2p energy levels of hierarchically structured $\text{Ni}_{0.75}\text{Cu}_{0.25}$ alloy. Insets in (d) are the HRTEM images and SAED pattern of $\text{Ni}_{0.75}\text{Cu}_{0.25}$ alloy.

all three samples, indicating that Ni and Cu are evenly distributed throughout the hierarchically structured Ni-Cu alloys. The corresponding XRD spectrum (Supporting Information, Figure S3) confirmed the {111} planes of the hierarchically structured Ni-Cu alloys are preferentially oriented. Recently, it has been reported that the {111} crystal planes of Cu and Ni have enhanced catalytic activity toward methanol oxidation.^[14] As seen in Figure 1 and the Supporting Information, Figure S1, the hierarchically structured Ni-Cu alloys composed of interconnected branches may allow the active {111} crystal plane to be fully exposed, which is favorable for the electrocatalytic oxidation reaction of methanol. For the XPS survey, peaks in the full XPS spectrum indicate the existence of Cu, Ni, O, and C elements (Figure 1 e; Supporting Information, Figure S6 a,c). The presence of C and O are most likely due to the contaminant hydrocarbon and the oxidation of freshly deposited product, respectively. XPS spectra of Cu 2p and Ni 2p regions of hierarchically structured $\text{Ni}_{0.75}\text{Cu}_{0.25}$ sample shown in Figure 1 f reveal that the surface of the product is covered with metallic ions as well as predominant oxygen species (as evidenced by the very strong O signals) rather than metallic atoms.

On the basis of the electrodeposition profiles (Supporting Information, Figure S8) and FESEM images (Supporting Information, Figure S9), the formation mechanism involving the seeding growth of branched Ni-Cu alloys are illustrated in Figure 2. First, Ni^{2+} and Cu^{2+} ions in the solution are rapidly

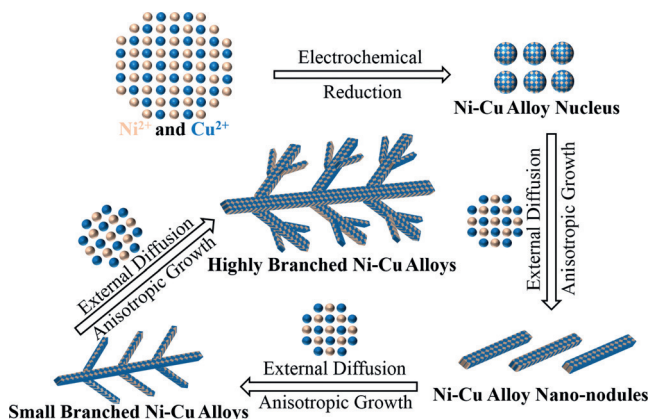


Figure 2. Illustration of the formation of highly branched Ni-Cu alloys. The growth of branch may be attributed to nuclei moving in random walk trajectories and sticking on a seed particle with tips growing preferentially.

electrochemically reduced into the isolated Ni-Cu alloy nucleus on Ti substrates. These nuclei (that is, Ni-Cu alloy nanoparticles) were uniformly and randomly distributed (upper right panel in Figure 2; Supporting Information, Figure S9a). As the deposition time increases, the isolated nuclei develop into Ni-Cu alloy nano-nodules (lower right panel in Figure 2; Supporting Information, Figure S9b) owing to the diffusion-limited growth process^[15] as a result of the concentration gradient of Ni^{2+} and Cu^{2+} ions in the solution. These nano-nodules serve as the growth sites or seeds. The subsequent growth of Ni-Cu alloy crystals preferentially occur on the formed nano-nodules rather than on the surface of Ti substrate, which is probably due to the relatively high activation energy for the surface reaction,^[16] thereby facilitating an anisotropic growth to yield branched alloys with nanofeelers on each branch (lower left panel in Figure 2), and finally grow into highly branched, hierarchically structured Ni-Cu alloys (middle panel in Figure 2; Supporting Information, Figure S9c,d). As noted above, the application of higher current densities promoted a vigorous hydrogen evolution and thus resulted in a diffusion-controlled deposition process. The agitation of the solution that is due to hydrogen generation resulted from the large applied current density limited the mass-transfer of Ni-Cu clusters formed locally in the solution to the Ti substrates, leading to diffusion-limited aggregation^[15] and thus forming the branched Ni-Cu alloy networks. This diffusion-limited aggregation is clearly evidenced by comparing the different structures of Ni-Cu alloys by varying the deposition temperature (Supporting Information, Figure S10 and Figure S11) and current density (Supporting Information, Figure S12 and Figure S13).

These highly branched, hierarchically structured Ni-Cu alloys carry the following advantageous characteristics: the

large electrochemically active surface area and porous structures due to branching, which are highly desirable for electrocatalytic applications. Figure 3a compares cyclic voltammograms of the $\text{Ni}_{0.75}\text{Cu}_{0.25}$, $\text{Ni}_{0.50}\text{Cu}_{0.50}$, and $\text{Ni}_{0.25}\text{Cu}_{0.75}$ alloys with the potential ranging from -0.1 V to $+1.0$ V in

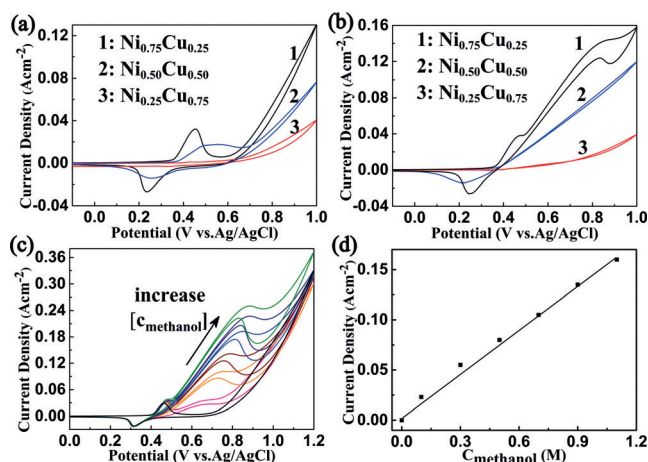


Figure 3. a) Cyclic voltammograms of hierarchically structured Ni-Cu alloys in 1.0 M NaOH solution at a scan rate of 50 mVs^{-1} . b) Cyclic voltammograms of hierarchically structured Ni-Cu alloys for methanol electrooxidation in 1.0 M NaOH solution at a scan rate of 50 mVs^{-1} . c) Cyclic voltammograms for hierarchically structured $\text{Ni}_{0.75}\text{Cu}_{0.25}$ alloys in 1.0 M NaOH solution in the presence of different concentrations of methanol (0.0, 0.1, 0.3, 0.5, 0.7, 0.9, and 1.1 M) at a scan rate of 50 mVs^{-1} . d) Relationship between the oxidation peak current density (the baseline current obtained in NaOH is subtracted) and the concentrations of methanol.

1.0 M NaOH solution at a scan rate of 50 mVs^{-1} . For the $\text{Ni}_{0.75}\text{Cu}_{0.25}$ sample, peaks at $+0.43$ V in a forward scan corresponding to Ni^{II} oxidation and at $+0.23$ V in a backward scan corresponding to Ni^{III} reduction can be observed, which can be ascribed to the $\text{Ni}^{\text{II}}/\text{Ni}^{\text{III}}$ transformation in the anodic and the cathodic sweep, respectively. The cyclic voltammogram of the $\text{Ni}_{0.50}\text{Cu}_{0.50}$ electrode is obviously different from that of the $\text{Ni}_{0.75}\text{Cu}_{0.25}$ electrode, displaying wider peaks for both the anodic peak at $+0.54$ V and a corresponding cathodic peak at $+0.25$ V. In the case of the $\text{Ni}_{0.25}\text{Cu}_{0.75}$ electrode, the weak electrochemical response with negligible $\text{Ni}^{\text{II}}/\text{Ni}^{\text{III}}$ redox peaks related to the oxide/hydroxide was observed, which may be attributed to the lower Ni content and the lower electrochemical activity of Cu when compared with Ni. The oxidation peak current density of Ni^{II} at the $\text{Ni}_{0.75}\text{Cu}_{0.25}$ electrode is 32 mA cm^{-2} and higher than that of the $\text{Ni}_{0.50}\text{Cu}_{0.50}$ (18 mA cm^{-2}) electrode (Figure 3a). On the other hand, the onset oxidation potential of the $\text{Ni}_{0.75}\text{Cu}_{0.25}$ and $\text{Ni}_{0.50}\text{Cu}_{0.50}$ electrodes were estimated to be $+0.35$ V and $+0.37$ V, respectively, indicating that the $\text{Ni}_{0.75}\text{Cu}_{0.25}$ electrode had the fastest electrochemical response in 1.0 M NaOH solution among all Ni-Cu alloyed electrodes. Notably, the oxidation peaks for the $\text{Ni}_{0.75}\text{Cu}_{0.25}$ and $\text{Ni}_{0.50}\text{Cu}_{0.50}$ electrodes were shifted to a higher position ($+0.43$ V and $+0.54$ V) and the corresponding reduction peaks were shifted to a lower position ($+0.23$ V and $+0.25$ V) compared to those of Ni

(+0.40 V for the oxidation peak and +0.30 V for the reduction peak) that were previously reported.^[17] This may be due to the alloyed structure and composition of the Ni-Cu samples.

Obviously, the electrochemical response of the Ni_{0.75}Cu_{0.25} electrode is much faster than that of the Ni_{0.25}Cu_{0.75} and Ni_{0.50}Cu_{0.50} electrodes (Figure 3a). Thus the surface coverage of Ni^{II}/Ni^{III} redox species (Γ^*) in the Ni_{0.75}Cu_{0.25} electrode was studied (Supporting Information, Figure S14). The value of Γ^* for the Ni_{0.75}Cu_{0.25} electrode was calculated to be $4.48 \times 10^{-7} \text{ mol cm}^{-2}$ according to the average of the anodic and the cathodic results (Supporting Information, Figure S14b). For comparison, the Γ^* values for the Ni_{0.50}Cu_{0.50} and Ni_{0.25}Cu_{0.75} electrodes were found to be $2.36 \times 10^{-7} \text{ mol cm}^{-2}$ and $3.27 \times 10^{-8} \text{ mol cm}^{-2}$, respectively. The Γ^* value of pure Ni electrode ($7.78 \times 10^{-8} \text{ mol cm}^{-2}$) was also obtained under the same preparation condition.^[17] Clearly, it is not surprising that the Ni_{0.75}Cu_{0.25} electrocatalyst had a significantly higher oxidation peak current density owing to the larger surface coverage of redox species Γ^* , which is approximately 5-, 5-, and 9-fold higher than that calculated for the Ni/C-30 ($8.9 \times 10^{-8} \text{ mol cm}^{-2}$) electrode, the Ni/mesoporous silica ($8.9 \times 10^{-8} \text{ mol cm}^{-2}$) electrode, and the bulk nickel electrode ($6.04 \times 10^{-8} \text{ mol cm}^{-2}$), respectively.^[18] It has been reported that the Ni^{II}/Ni^{III} redox process is controlled by the solid-phase body of the proton diffusion.^[17b, 18c] Therefore, the diffusion coefficient (D) of the rate-limiting proton is an important parameter for characterization of the oxidation behavior of electrocatalysts. The D was found to be $2.89 \times 10^{-8} \text{ cm}^2 \text{ s}^{-1}$ for the Ni_{0.75}Cu_{0.25} electrode (Supporting Information, Figure S14c). It is important to note that this D value is far more than the reported values on the nanoporous Ni-Cu-P alloy ($3.65 \times 10^{-10} \text{ cm}^2 \text{ s}^{-1}$) and the Ni-B nanoparticles modified nanoporous Cu electrode ($4.81 \times 10^{-9} \text{ cm}^2 \text{ s}^{-1}$).^[18c, 19] Moreover, this D value is also 3 times and more than two orders of magnitude higher than the Ni_{0.50}Cu_{0.50} and Ni_{0.25}Cu_{0.75} electrodes ($8.63 \times 10^{-9} \text{ cm}^2 \text{ s}^{-1}$ and $1.34 \times 10^{-10} \text{ cm}^2 \text{ s}^{-1}$, respectively). As seen in Figure 3a, the more negative onset oxidation potential of the Ni_{0.75}Cu_{0.25} electrode than that of the Ni_{0.50}Cu_{0.50} and Ni_{0.25}Cu_{0.75} electrodes at the same scan rate may be ascribed to the much larger D value.

Figure 3b compares cyclic voltammograms of the Ni_{0.75}Cu_{0.25}, Ni_{0.50}Cu_{0.50}, and Ni_{0.25}Cu_{0.75} electrodes for MOR in 1.0 M NaOH solution with 0.5 M methanol at the scan rate of 50 mV s^{-1} . It is clear that the Ni_{0.50}Cu_{0.50} and Ni_{0.25}Cu_{0.75} electrodes displayed a mildly increased oxidation current density. In sharp contrast, the Ni_{0.75}Cu_{0.25} electrode demonstrated a markedly enhanced anodic peak at +0.83 V (vs. Ag/AgCl), reflecting 7 times higher current density for MOR compared to that using the Ni_{0.25}Cu_{0.75} electrode at the same potential. Obviously, the Ni_{0.75}Cu_{0.25} electrode exhibited a significantly higher electrocatalytic activity, signifying that the highly branched hierarchical structures together with the proper Ni/Cu atomic ratio can greatly enhance the electrochemical activity of the Ni_{0.75}Cu_{0.25} catalyst for MOR. The hierarchical structure of highly branched Ni-Cu alloy networks combined with abundant pores (marked in Figure S9c, S9d in the Supporting Information) achieved by hydrogen evolution-assisted electrodeposition approach that creates

extremely rough surface can provide a larger electrochemical active area (ECSA), which was evaluated from electrochemical double-layer capacitance (C_{dl}). An ECSA of 112.5 cm^2 was found in Ni_{0.75}Cu_{0.25}, which is higher than that of Ni_{0.50}Cu_{0.50} (90 cm^2) and Ni_{0.25}Cu_{0.75} (72.5 cm^2 ; Supporting Information, Figure S15). Along with high surface area of the porous structure, the electron transfer from Ni to Cu^[20] leading to the depletion of electrons and the increase of the oxidation state of Ni may accelerate the methanol oxidation and largely improve the electrocatalytic activity of Ni_{0.75}Cu_{0.25}. A catalytic performance comparison between Ni_{0.75}Cu_{0.25} and other reported non-noble metal as well as the commercial Pt/C and PtRu/C catalysts for MOR is summarized in the Supporting Information, Tables S2 and S3. It is important to note that the hierarchically structured Ni_{0.75}Cu_{0.25} alloy clearly outperforms other existing MOR non-noble metal catalysts, despite that it still cannot exceed the commercial Pt-based catalysts.

Although the use of highly concentrated methanol solution in DMFCs is preferable as it improves the power density and simultaneously diminishes the cell size, the application of absolute methanol is impossible as water is a reactant in the process of MOR. Thus, the methanol concentration is an important variable for MOR. Figure 3c displays the correlation between the methanol concentration and the electrocatalytic activity of the Ni_{0.75}Cu_{0.25} electrode at a sweep rate of 50 mV s^{-1} . The oxidation peak current density for the Ni_{0.75}Cu_{0.25} electrode in the presence of 0.1 M methanol increased largely, contrasting sharply with the absence of methanol in 1.0 M NaOH solution. With the increase of the methanol concentration, the oxidation peak potential exhibited a positive shift, indicating that methanol molecules adsorbed on the electrocatalyst surface can be oxidized at higher potentials compared to the oxidation of Ni^{II} to Ni^{III}. Moreover, the anodic peak current in the positive scan was proportional to the methanol concentration, and the increase in the methanol concentration caused a nearly proportional enhancement of the anodic peak current density (Figure 3d). This linear relationship between anodic current density and methanol concentration substantiated that the methanol oxidation process is controlled by the diffusion of methanol. Furthermore, it was found that the current density rose with the increase of the methanol concentration at the initial stage of the cathodic sweep, signifying that methanol molecules and their oxidation intermediates on the surface of electrocatalysts cannot be completely oxidized in the anodic scan and have to continue to be oxidized at the high potential in the cathodic scan. Interestingly, the anodic current passed through a maximum as the potential was anodically swept (Figure 3c) owing to the fact that the number of active sites for methanol adsorption tends to decrease. In the reverse half cycle, the oxidation continued and its corresponding current went through a maximum (Figure 3c) owing to the regeneration of active adsorption sites for methanol as a result of the removal of adsorbed intermediates and products.

Chronoamperometry was also used to further determine the long-term activity and stability of the Ni-Cu alloy electrocatalysts for MOR. Figure 4 compares the chronoamperograms obtained from the Ni_{0.75}Cu_{0.25}, Ni_{0.50}Cu_{0.50}, and

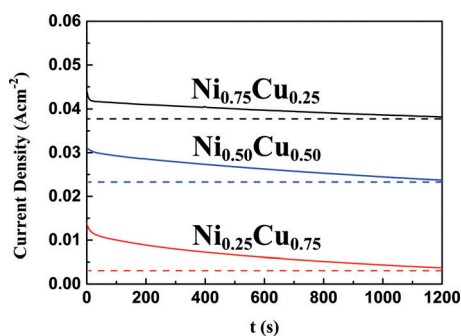


Figure 4. Chronoamperograms of hierarchically structured Ni-Cu alloys in the presence of 0.5 M methanol in 1.0 M NaOH solution at a potential step of +0.65 V for 1200 s.

Ni_{0.25}Cu_{0.75} electrodes, respectively, in 1.0 M NaOH solution containing 0.5 M methanol at a potential step of +0.65 V for 1200 s. Clearly, the current densities sharply dropped at the beginning and then slightly decreased for all three electrodes. At the beginning of the reaction, it is a fast kinetic reaction so the active sites are free of adsorbed methanol molecules. After that, the adsorption of new methanol molecules depends on the liberation of the electrocatalytic sites via methanol oxidation or of the intermediate species such as CO, CH_x, and CH₃O formed during the first several minutes (a rate-determining step) that are responsible for the poisoning of the active sites.^[21] Therefore, the slightly decreased current density may be due primarily to the poisoning of the catalysts. Furthermore, it is obvious that the attenuation of the current for the Ni_{0.75}Cu_{0.25} electrode was relatively slower than that for the Ni_{0.50}Cu_{0.50} and Ni_{0.25}Cu_{0.75} electrodes (representing in the difference between the solid and dotted lines in Figure 4), implying that the Ni_{0.75}Cu_{0.25} electrode possesses a higher stability than the Ni_{0.50}Cu_{0.50} and Ni_{0.25}Cu_{0.75} electrodes toward MOR. Moreover, the average current density for the Ni_{0.75}Cu_{0.25} electrode (40 mA cm⁻²) increased by several times compared to that for the Ni_{0.50}Cu_{0.50} (27 mA cm⁻²) and Ni_{0.25}Cu_{0.75} (7 mA cm⁻²) electrodes, suggesting that the Ni_{0.75}Cu_{0.25} electrode is more active, which is consistent with the cyclic voltammetry results (Figure 4).

In summary, we developed a viable hydrogen evolution assisted electrodeposition strategy to craft highly branched, hierarchical structured Ni-Cu alloy networks with large surface areas and porous space within network. The preferentially oriented {111} planes in the resulting Ni-Cu alloys render the enhanced electrocatalytic oxidation of methanol. Such highly branched Ni-Cu structures are formed due to the diffusion-limited aggregations of Ni-Cu clusters formed locally in the solution. Among three hierarchical structured Ni-Cu alloys produced, the electrochemical response of Ni_{0.75}Cu_{0.25} is much faster than that of Ni_{0.25}Cu_{0.75} and Ni_{0.50}Cu_{0.50}. As an electrocatalyst for methanol oxidation in alkaline solution, the Ni_{0.75}Cu_{0.25} electrode exhibits a larger peak current density of 140 mA cm⁻² and a long-term chronoamperometry stability, thereby leading to excellent electrocatalytic activity toward methanol oxidation. This work may represent a significant advance in crafting inexpensive bimetallic alloys containing earth-abundant elements

for high-efficiency electrocatalysts and is an important step toward the pursuit of affordable and efficient DMFCs.

Acknowledgements

This work was financially supported by the Chongqing University Postgraduates' Innovation Project (2015) and the Fundamental Research Funds for the Central Universities (Project No. 106112015CDJZR305501). X.C. acknowledges the financial support from the China Scholarship Council.

Conflict of interest

The authors declare no conflict of interest.

Keywords: electrocatalysis · electrodeposition · hierarchical structures · methanol oxidation · Ni-Cu alloy

How to cite: *Angew. Chem. Int. Ed.* **2017**, *56*, 4488–4493
Angew. Chem. **2017**, *129*, 4559–4564

- [1] N. Kakati, J. Maiti, S. H. Lee, S. H. Jee, B. Viswanathan, Y. S. Yoon, *Chem. Rev.* **2014**, *114*, 12397–12429.
- [2] a) X. Lu, Z. Deng, C. Guo, W. Wang, S. Wei, S.-P. Ng, X. Chen, N. Ding, W. Guo, C.-M. L. Wu, *ACS Appl. Mater. Interfaces* **2016**, *8*, 12194–12204; b) J. Rossmeisl, P. Ferrin, G. A. Tritsarlis, A. U. Nilekar, S. Koh, S. E. Bae, S. R. Brankovic, P. Strasser, M. Mavrikakis, *Energy Environ. Sci.* **2012**, *5*, 8335–8342; c) X. Zhao, M. Yin, L. Ma, L. Liang, C. Liu, J. Liao, T. Lu, W. Xing, *Energy Environ. Sci.* **2011**, *4*, 2736–2753.
- [3] a) A. Ahmadi Daryakenari, D. Hosseini, Y.-L. Ho, T. Saito, A. Apostoluk, C. R. Müller, J.-J. Delaunay, *ACS Appl. Mater. Interfaces* **2016**, *8*, 15975–15984; b) J. Yang, J. Tan, F. Yang, X. Li, X. Liu, D. Ma, *Electrochem. Commun.* **2012**, *23*, 13–16; c) N. A. Barakat, M. Motlak, A. A. Elzatahry, K. A. Khalil, E. A. Abdelghani, *Int. J. Hydrogen Energy* **2014**, *39*, 305–316.
- [4] a) S. De, J. Zhang, R. Luque, N. Yan, *Energy Environ. Sci.* **2016**, *9*, 3314–3347; b) N. A. Barakat, M. Motlak, *Appl. Catal. B* **2014**, *154*, 221–231; c) I. Danaee, M. Jafarian, A. Mirzapoor, F. Gopal, M. Mahjani, *Electrochim. Acta* **2010**, *55*, 2093–2100.
- [5] a) T. Frelink, W. Visscher, J. Van Veen, *Surf. Sci.* **1995**, *335*, 353–360; b) M. A. Watanabe, S. Motoo, *J. Electroanal. Chem.* **1975**, *60*, 267–273.
- [6] a) W. Guo, W. Q. Tian, X. Lian, F. Liu, M. Zhou, P. Xiao, Y. Zhang, *Comput. Theor. Chem.* **2014**, *1032*, 73–83; b) Q. Jiang, L. Jiang, H. Hou, J. Qi, S. Wang, G. Sun, *J. Phys. Chem. C* **2010**, *114*, 19714–19722.
- [7] Y. Ding, M. Chen, J. Erlebacher, *J. Am. Chem. Soc.* **2004**, *126*, 6876–6877.
- [8] H. Huang, X. Wang, *J. Mater. Chem. A* **2014**, *2*, 6266–6291.
- [9] F. Bai, Z. Sun, H. Wu, R. E. Haddad, X. Xiao, H. Fan, *Nano Lett.* **2011**, *11*, 3759–3762.
- [10] a) P. Trogadas, V. Ramani, P. Strasser, T. F. Fuller, M. O. Coppens, *Angew. Chem. Int. Ed.* **2016**, *55*, 122–148; *Angew. Chem.* **2016**, *128*, 128–156; b) J. Wang, Y. Zhong, L. Wang, N. Zhang, R. Cao, K. Bian, L. Alarid, R. E. Haddad, F. Bai, H. Fan, *Nano Lett.* **2016**, *16*, 6523–6528.
- [11] a) X. Huang, Y. Li, Y. Chen, E. Zhou, Y. Xu, H. Zhou, X. Duan, Y. Huang, *Angew. Chem. Int. Ed.* **2013**, *52*, 2520–2524; *Angew. Chem.* **2013**, *125*, 2580–2584; b) B. Lim, Y. Xia, *Angew. Chem. Int. Ed.* **2011**, *50*, 76–85; *Angew. Chem.* **2011**, *123*, 78–87; c) A.

- Mohanty, N. Garg, R. Jin, *Angew. Chem. Int. Ed.* **2010**, *49*, 4962–4966; *Angew. Chem.* **2010**, *122*, 5082–5086.
- [12] a) S. Gheorghiu, M. O. Coppens, *AIChE J.* **2004**, *50*, 812–820; b) B. Zhao, M. M. Collinson, *Chem. Mater.* **2010**, *22*, 4312–4319.
- [13] a) S. Cherevko, N. Kulyk, C.-H. Chung, *Langmuir* **2012**, *28*, 3306–3315; b) W. Huang, M. Wang, J. Zheng, Z. Li, *J. Phys. Chem. C* **2009**, *113*, 1800–1805.
- [14] a) R. Venkatasubramanian, J. He, M. W. Johnson, I. Stern, D. H. Kim, N. S. Pesika, *Langmuir* **2013**, *29*, 13135–13139; b) M. Zhou, P. Xiao, W. Guo, J. Deng, F. Liu, Y. Zhang, *J. Electrochem. Soc.* **2014**, *161*, H133–H137.
- [15] T. Witten, Jr., L. M. Sander, *Phys. Rev. Lett.* **1981**, *47*, 1400.
- [16] Y. Qin, Y. Song, N. Sun, N. Zhao, M. Li, L. Qi, *Chem. Mater.* **2008**, *20*, 3965–3972.
- [17] a) X. Cui, W. Guo, M. Zhou, Y. Yang, Y. Li, P. Xiao, Y. Zhang, X. Zhang, *ACS Appl. Mater. Interfaces* **2015**, *7*, 493–503; b) X. Cui, Y. Yang, Y. Li, F. Liu, H. Peng, Y. Zhang, P. Xiao, *J. Electrochem. Soc.* **2015**, *162*, F1415–F1424.
- [18] a) R. A. Hameed, R. M. El-Sherif, *Appl. Catal. B* **2015**, *162*, 217–226; b) S. N. Azizi, S. Ghasemi, E. Chiani, *Electrochim. Acta* **2013**, *88*, 463–472; c) S.-J. Zhang, Y.-X. Zheng, L.-S. Yuan, L.-H. Zhao, *J. Power Sources* **2014**, *247*, 428–436.
- [19] L.-S. Yuan, Y.-X. Zheng, M.-L. Jia, S.-J. Zhang, X.-L. Wang, C. Peng, *Electrochim. Acta* **2015**, *154*, 54–62.
- [20] J.-E. Lim, S. H. Ahn, J. H. Jang, H. Park, S.-K. Kim, *Bull. Korean Chem. Soc.* **2014**, *35*, 2019.
- [21] E. Antolini, *Appl. Catal. B* **2007**, *74*, 337–350.

Manuscript received: February 1, 2017

Final Article published: March 23, 2017